FRACTOGRAPHY OF FATIGUE CRACK GROWTH IN LOW-ALLOY STEELS

J. Woodtli-Folprecht, M. Prodan** and J. C. Radon**

**Swiss Federal Laboratories for Materials Testing and Research, 8600 Dubendorf, Switzerland*
***Motor Columbus, 5401 Baden, Switzerland*
****Imperial College of Science and Technology, London, England*

ABSTRACT

The fatigue crack growth characteristics of two low-alloy steels were studied in terms of low frequency tensile cycling and of the fractography of part-through semi-elliptical cracks. Three microstructural processes were analysed: growth of crystallographic facets, striation formation, and ductile tearing. It was shown that the formation of striations does not describe fatigue crack growth sufficiently and other processes will have to be considered in a detailed cyclic crack growth analysis.

KEYWORDS

Fatigue crack growth; facets; striations; testing; micromechanisms of fatigue.

INTRODUCTION

The correct assessment of the propagation of microcracks formed in the plastic zone ahead of the crack tip is highly significant in the study of fatigue processes. The examination of separate micromechanisms relevant to cyclic crack propagation forms an essential part of our understanding of this subject. The fatigue crack growth characteristics of a range of Al-alloys were recently reported (1) and a number of individual mechanisms operating in the cyclic deformation was discussed. Three microprocesses were found to be of particular importance for crack extension in Al-alloys and their combined effect was considered in the evaluation of the observed macroscopic crack growth behaviour. These processes were: cleavage of the matrix, often environmentally embrittled; formation of striations; and coalescence of microvoids.

A similar approach may be adopted in the study of the cyclic deformation of structural steels. Because of the economic importance of these materials, a detailed understanding of fatigue crack growth is necessary. The two structural steels chosen for this work have frequently been specified for the fabrication of very large engineering structures, such as offshore oil platforms, where a high resistance to fatigue failure is required.

MATERIALS

The test materials selected were weldable structural steels, Table 1. The tensile plate specimens were made from steel BH 43W and the four-point bend specimens from BS4360-50D. The typical microstructure of the 50D steel, consisting of ferrite and pearlite, is shown in Fig. 1. The microstructure and grain size of the second steel, BH 43W, was very similar in appearance. The grain size of both materials corresponded to ASTM (E112) Class 9. The mean diameter of the grains was 10 to 15μm.

SPECIMENS AND TEST PROCEDURE

Part-through cracks are frequently encountered in welded structures. These cracks are usually found in weld material or in HAZ, but their growth may often be rather complicated. After the initiation in HAZ, the cracks propagate through the parent metal and, consequently, the analysis of the crack growth involves at least a duplex material. In the present tests only parent material results are reported.

The fatigue tests were carried out on precracked plates provided with sharp, semi-elliptical surface notches. The dimensions of the tensile specimens were 20 mm x 150 mm x 800 mm with a central starter notch, a = 2 mm and $2c$ = 14 mm. These were tested in a 1000 kN Amsler loading frame at 6 Hz. The four-point bend specimens were tested at 30 Hz in a specially built Dartec 200 kN electrohydraulic machine. The dimensions of the bend specimens were 25.4 mm x 111 mm x 450 mm with a starter notch, a = 5.5 mm and $2c$ = 40mm. Both types of specimens were cut with their longitudinal axes in the direction of rolling.

After testing, the specimens were broken in liquid nitrogen and the fatigue fracture surfaces examined in a SEM. Striation spacings were compared with macroscopically determined crack growth rates and plotted as functions of da/dN versus ΔK.

CALCULATIONS OF CRACK GROWTH RATES

The method for computing da/dN and dc/dN involves fitting second-order polynomials to successive sets of measured (N, a) and (N, c) data points. a, c and N are the respective notations for crack depth, half crack length and cycle numbers.

The associated values of ΔK were computed using the Finite Element solution of Raju and Newman (6)

$$F\left(\frac{a}{c}, \Psi, \frac{a}{t}\right) = \frac{K.\ \Phi}{\sigma.\sqrt{\Pi a}}$$

for the tensile plates. F, Ψ, t, K, Φ and σ are the respective notations for the correction function, polar co-ordinate angle, thickness, stress intensity factor, elliptical integral second kind and normal stress. The ΔK values for the plates subjected to bending were estimated using the calibration equation of Koterazawa and Minamisaka combined with a correction function (7).

FRACTOGRAPHY

Figure 2 shows a number of crystallographic facets in the proximity of the notch base. These facets initiated along the suitably orientated slip planes; it is suggested that their star-like shapes indicate that they were formed by sudden bursts just under the notch surface, probably not lower than 0.2 mm below the base of the notch.

Figures 3 and 4 show typical records of fracture surface topography near to the notch root. The fracture surface is very uneven and a high degree of irregularity in the growth of singular fatigue paths is clearly apparent. Some of these paths are covered with very fine fatigue striations. The fatigue paths are numerous and their distribution suggests a frequent, but localised, initiation of fatigue cracks. This behaviour is similar for both materials at short crack lengths; for 50D steel, a = 7.5 mm Fig. 3, and for BH 43W, a = 3mm Fig. 4. As described by Laird (3) and others (4), the striations in Fig. 5 are typically "ductile". They are evenly spaced, covering the whole surface of individual fatigue paths, which extend over an area of a large number of grains. With the increasing length of the fatigue crack, the density of the striations is noticeably decreasing and the number of other morphological features, such as secondary cracks and dimples, is increasing.

Two types of secondary cracks can be observed. The large, widely open cracks were coarse, Fig. 6. These cracks (arrow 1) were often the result of a separation at the grain boundaries. However, similar coarse cracks were also found at the non-metallic inclusions, Fig. 7. All coarse cracks were independent of the overall crack propagation direction. The fine secondary cracks ran parallel to the fatigue striations, Fig. 6, arrow 2.

The depth of the secondary cracks depends mostly on their orientation. The coarse cracks situated on the grain boundaries ran generally to the depth of one grain, while the fine cracks were relatively shallow and not deeper than 5 μm. On the other hand, the secondary cracks which initiated at the non-metallic inclusions, were comparatively deep and, depending on the orientation, they may follow the rows of inclusions, where the branching of the main crack often occurs, as in Fig. 7.

Fig. 8 shows a stepped facet in 50D steel. This is a typical characteristic of fractures in the vicinity of non-metallic inclusions and also at lower values of ΔK. Geometrically similar, but larger facets were observed on crossing the pearlite bands and the arrow 1 in Fig. 8 indicates the focus of an isolated burst, macroscopically recorded on the AC potential drop record. Bursts of this type occurred in the $\Psi = \pi/2$ direction, approximately 0.5 mm long, initiating at an inclusion (arrow 2).

In region II of the da/dN versus ΔK curve, a high density of the secondary cracks was observed in the area of the beach marks. This increasing crack density was noted in both steels and confirms the previous observation on boiler steels (2). In general, the crack runs along the secondary cementite at the ferritic grain boundaries, or through the pearlitic colony, Fig. 9. More importantly, the number of morphological features of tearing increases with the increasing ΔK value, and this was particularly obvious in the $\Psi = 0$ direction.

CORRELATION OF MICROSCOPIC AND MACROSCOPIC CRACK GROWTH RATES

The experimental data obtained in fatigue tests can be conveniently compared with those derived from the measurement of striation spacing. An example of such correlations is shown in Fig. 10 for the tensile fatigue tests performed on steel BH 43W. The results presented include the upper transition,

together with a part of regions II and III. It will be observed that the striation spacings at the ΔK values of 20 MPa $m^{\frac{1}{2}}$ agree substantially with the direct observation of the crack growth. However, at ΔK values in the region of 30 MPa $m^{\frac{1}{2}}$ and higher, a marked difference may be noted. The present results demonstrate a good one-to-one correspondence between cycles and striations in region II. At higher ΔK values, where there is an increased amount of ductile tearing, the striation spacing is significantly less than da/dN. Cycling at low ΔK values may substantially decrease the number of striations. At still lower ΔK, the continuum considerations of the crack growth will not be applicable.

DISCUSSION

It is commonly accepted that the fatigue crack propagation process can be simply described by a relationship of the form da/dN = a simple function of ΔK, such as proposed by Rice (8) and others (9). However, crack growth rate measurements presented in this work indicate without doubt that, while this simple relation describes the crack growth in a limited ΔK region, usually defined as region II quite satisfactorily, it can not be used for all ΔK values indiscriminately. It has been observed that at very high ΔK values, the macroscopic growth is substantially higher than expected and, in fact, also higher than that calculated from the microscopic observations of the striation spacings. Conversely, the growth rate is very much lower than expected in fatigue at very low values of ΔK. Such changes in the crack propagation rate were recently reported on boiler steel H1 described in (2) and also on a range of Al-alloys (1, 10).

The SEM observations discussed above indicate three modes of cyclic crack propagation. At very low values of ΔK and in the laboratory air environment at 30 Hz and $R = 0.1$, the fatigue fracture surface showed predominantly crystallographic facets. This regime is usually described as the threshold region, and the minimum value of ΔK_{TH}, averaged for all thicknesses of the 50D steel, was 2.9 MPa $m^{\frac{1}{2}}$. Examination of the crack fronts at ΔK_{TH} revealed an almost entirely faceted fracture topography. These facets showed frequent steps and, in some cases, an appearance, albeit misleading, of striations. These facets, originally described by Forsyth (5) on smooth specimens, are mostly featureless, partly because of the extensive rubbing of the fractured surfaces and partly due to the limited resolutions of the SEM.

The second regime, region II, begins at a ΔK value of 10 MPa $m^{\frac{1}{2}}$ at a crack growth rate of 10^{-6} mm/cycle. Here a gradual change of the fracture surface was observed and typical fatigue striations noted. The crack growth rate can be represented by a crack propagation law of the form mentioned above. The striation spacing, measured by a well-established microscopic method, provided adequate crack growth rate data. In the present tests, the correlation between the striation spacing, optical surface crack length measurement and the electropotential AC method was excellent. The fatigue crack growth was transgranular, the path was relatively straight and the crack without any indication of significant branching; its direction was perpendicular to the applied stress.

At higher ΔK values from approximately 30 MPa $m^{\frac{1}{2}}$ at 10^{-4} mm/cycle, the number of striations increased only slightly; in this region III, the crack extended by a combination of fatigue striations and microvoid coalescence. The proportion of dimples increased with the increasing value of ΔK. A fully ductile fracture occurred at K_{max} close to the value of K_c. It was apparent that the dependence of the ductile fracture on K_{max} was stronger than on the

range of ΔK. Note that the change of R-ratio from 0.1 to 0.7 did not substantially influence the fracture mode, at least not in these two steels.

CONCLUSIONS

(i) A detailed analysis of fatigue crack propagation in low alloy steels was presented.

(ii) Three microstructural processes provide the basis of cyclic crack growth; these are:

(a) Growth of crystallographic facets.

(b) Formation of striations.

(c) Ductile tearing.

REFERENCES

(1) Rhodes, D., Nix, K.J., and Radon, J.C. (1982). Proc. 4th ECF Conf., (Leoben), 443-448.

(2) Woodtli-Folprecht, J. and Prodan, M. (1982). Proc. 4th ECF Conf., (Leoben) 480-487.

(3) Laird, C. (1966). ASTM STP 415, 131-168.

(4) Nix, K.J., and Flower, H.M. (1982). Acta Met., 30, 1549-1559.

(5) Forsyth, P.J.E. (1961). Symp. on Crack Propagation, Cranfield.

(6) Raju, I.S. and Newman, J.C., (1979). Engng. Fracture Mechanics, 11, 817.

(7) Koterazawa, R. and Minamisaka, S. (1977). Technical Notes: Stress Intensity Factors of Semi-elliptical Surface Cracks in Bending, Osaka University, Toyonaka/Japan, 915-921.

(8) Rice, J.R. (1967). Fatigue Crack Propagation. ASTM STP 413, 247-309

(9) Fine, M.E. and Ritchie, R.O. (1979). Fatigue and Microstructure. ASM, Metals Park, OH., 245-272.

(10) Rhodes, S.D., Nix. K.J. and Radon, J.C. (1984). Int. J. Fatigue, 6, 3-7.

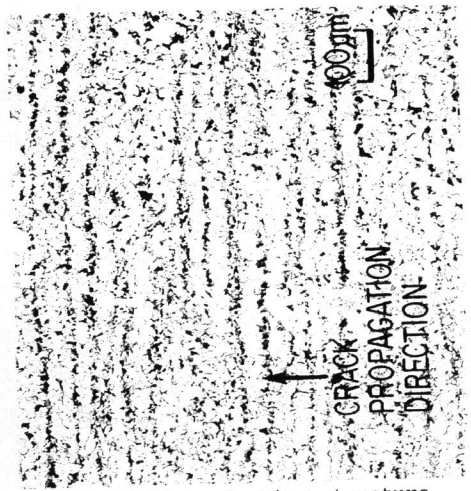

Fig. 1 BS 4360-50D. Microstructure

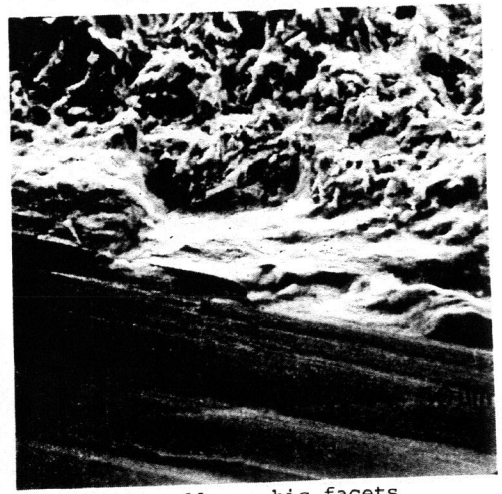

Fig. 2. Crystallographic facets.

TABLE 1 Chemical composition and mechanical properties

	C	Si	Mn	P	S	Nb	V	Ni
BS4360-50 D	≤0.18	<0.5	0.15	≤0.04	≤0.04	<0.1	<0.1	-
BH-43 W	0.18	0.32	1.38	0.017	0.009	-	0.17	0.61

	0,2% Proof stress (MPa)	Tensile strength (MPa)	Elongation A_5 (%)	Impact Strength (J)
50 D	388	563	20	-10°C:27
43 W	470	622	25	-20°C:65

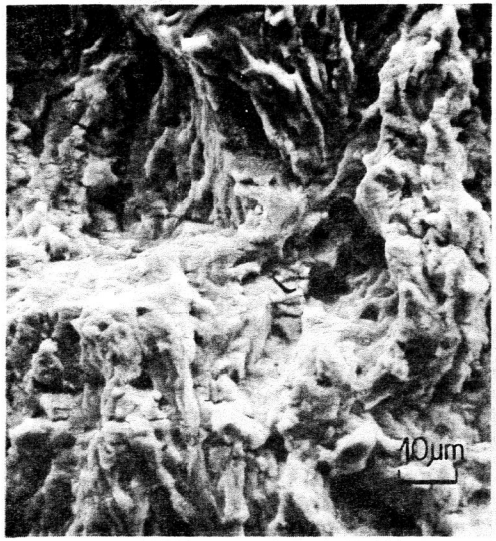

Fig. 3. 50D steel. a = 7.5 mm

Fig 4. BH 43W steel. a = 3 mm.

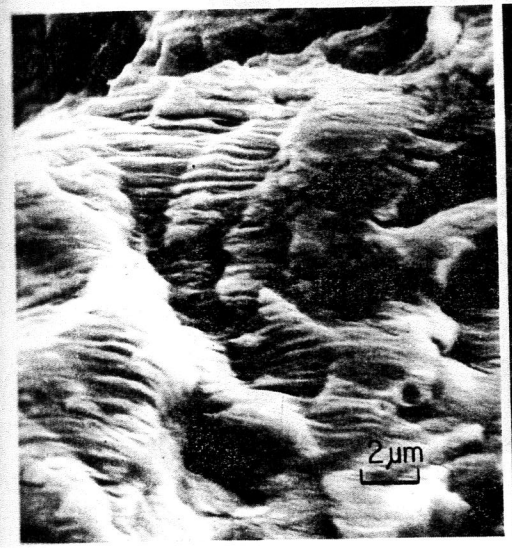

Fig. 5 Ductile striations

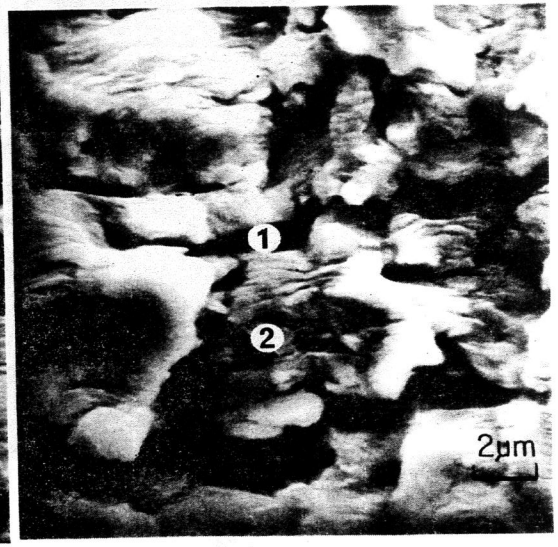

Fig. 6. Secondary cracks

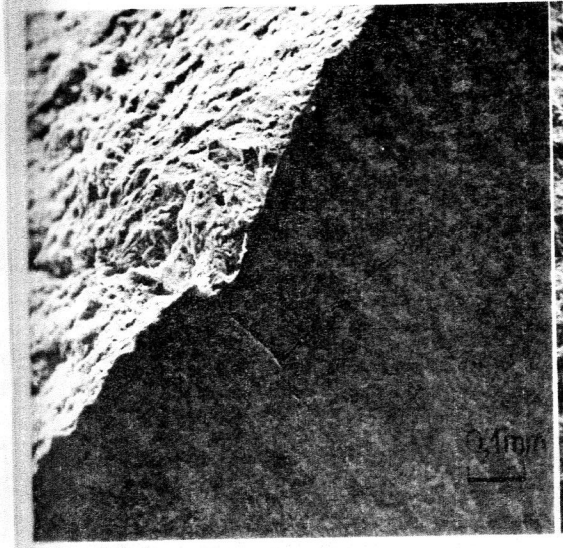

Fig. 7 Non-metallic inclusions

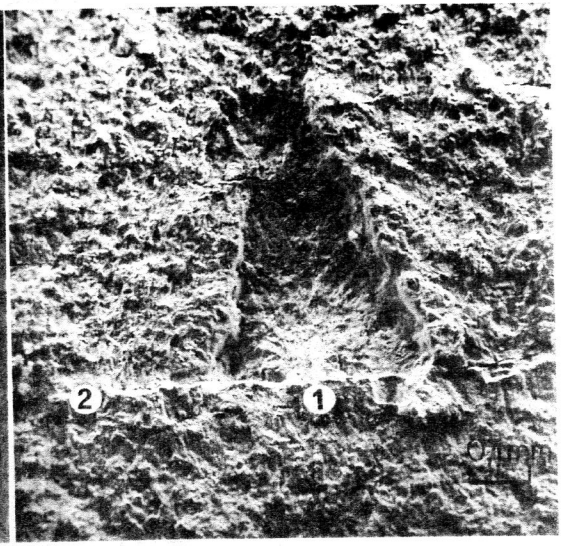

Fig. 8. A stepped facet

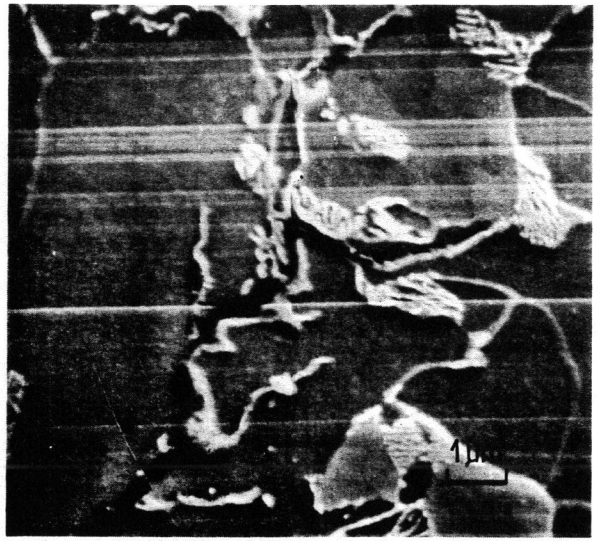

Fig. 9. A pearlitic colony

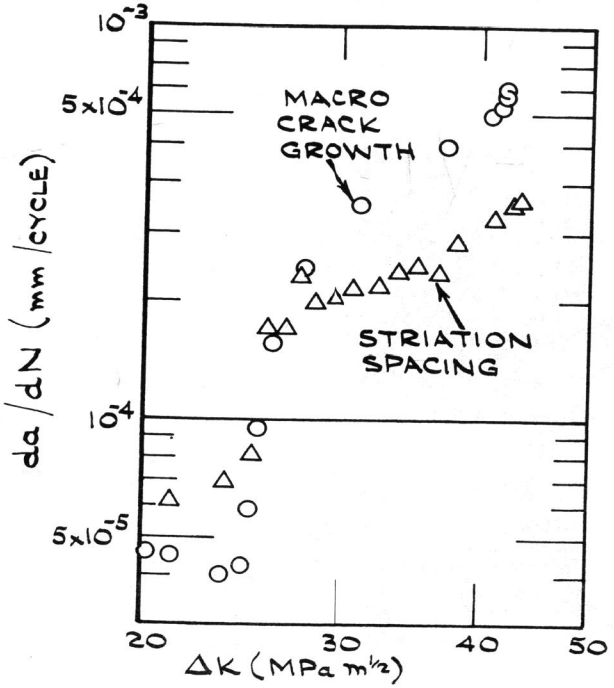

Fig. 10. 43W steel. *da/dN vs.* ΔK